Model-Based Analysis and Optimization of an ISPR Approach Using Reactive Extraction for Pilot-Scale L-Phenylalanine Production

R. Takors*

Institute of Biotechnology, Forschungszentrum Jülich GmbH, 52425 Jülich, Germany

Based on experimental data from fermentation runs, as well as from L-phenylalanine (L-Phe) separation studies, a simple model is presented that describes the total ISPR approach for on-line L-Phe separation. While fermentation process modeling via a macrokinetic model revealed an L-Phe inhibition constant of 20 ± 1.35 g/L using recombinant *E. coli* cells, the reactive-extraction process modeling identified the L-Phe cation diffusion in the aqueous donor film and the transport of the lowly soluble carrier/L-Phe complex in the aqueous acceptor film as the most dominant transfer steps. The corresponding mass transfer coefficients were estimated as $k_{PheD} = 128 \times 10^{-7}$ cm/s (extraction) and $k_{CPheA} = 178 \times 10^{-5}$ cm/s (back-extraction). Simulation studies were performed for the total ISPR approach, which gave hints for strategies of further process optimization.

Introduction

The aromatic amino acid L-phenylalanine (L-Phe) is of pharmaceutical importance for parenteral nutrition (Drauz et al., 2002) and represents a necessary building block for the production of the low-calorie sweetener aspartame, which is widely used in various foods and dry beverage mixes owing to its approximately 200-fold stronger sweetness compared to that of sucrose (Calorie Control Council, 2002). Today, worldwide L-Phe production is estimated to be 14,000 tons (Budzinski, 2001), which is expected to increase to sales of US$ 850 million in 2004 (Müller, 2001). Thus, L-Phe represents a typical fine chemical with a current market price of 20−40 US$/kg depending on its use for chemical or pharmaceutical purposes (Bongaerts et al., 2001).

For large-scale L-Phe production different routes are followed such as the resolution of *N*-acetyl-D,L-phenylalanine or the stereo- and enantioselective addition of ammonia to *trans*-cinnamic acid. However, it turned out that fermentation processes based on glucose-consuming L-Phe-producing mutants seem to be economically superior to the alternatives presented above (Drauz et al., 2002). In the past, a variety of L-Phe production processes have been developed (Bongaerts et al., 2001) using recombinant *Corynebacterium glutamicum*, *Brevibacterium flavum*, or *Lactofermentum* or *E. coli* strains. Among these, there is only one approach that aims at the on-line separation of the desired product, L-Phe, from the running fed-batch production process (Maass et al., 2002; Gerigk et al., 2002a). This in situ product removal (ISPR) was followed in order to minimize any inhibiting effect on the activity of AroF, one of the three isoenzymes of D-arabino-heptulusonate 7-phosphate (DAHP)-synthase, which catalyzes the precursor reaction to supply sufficient carbon to the aromatic amino acid pathway.

* Phone: +49/2461/613365. Fax: +49/2461/613870. E-mail: r.takors@fz-juelich.de.

As indicated in Figure 1, glucose was used as the sole carbon source. Additionally, L-tyrosine was fed to the process because L-tyrosine-auxotrophic, recombinant *E. coli* production strains were used. Both glucose and tyrosine were optimally controlled (Gerigk et al., 2002a; Gerigk et al., 2002b). For on-line L-Phe separation, a reactive-extraction approach was realized using kerosene as the organic solvent together with the cation-selective carrier DEHPA and sulfuric acid as the proton-counterion donor in the liquid acceptor phase. As a result, a 35% increase of the final L-Phe/glucose yield was achieved compared to the non-ISPR approach.

As presented in Gerigk et al. (2002a), approximately 2 kg of L-Phe was separated on-line during a pilot-scale 300 L production, while 5.5 kg of L-Phe was left in the suspension to be separated after the fermentation process had finished. Therefore, it was concluded that the ISPR approach holds great promise for further developments. Additional mass transfer studies were planned to investigate why only 26.7% of L-Phe could be separated on-line and how this potential limitation could be overcome experimentally. As a consequence, a simple model of the total ISPR pilot-scale process should be formulated to enable corresponding simulation studies. The process of modeling building, underlying assumptions, and simulation results will be presented in the following. Basic constraints for further process development are derived from simulation analysis.

Material and Methods

Biological System. The genetically engineered L-Phe production strain *E.coli* W3110-4(pF20), a derivative of *E. coli* K12, contains a chromosomal deletion Δ(*pheA tyrA aroF*) regarding *pheA* (coding for chorismate mutase/prephenate dehydratase), *tyrA* (coding for chorismate mutase/prephenate dehydrogenase), and *aroF* (coding for the tyrosine-sensitive DAHP synthase (2-desoxy-D-arabino-heptusonate 7-phosphate). Besides tyrosine ($aroF^{fbr}$) and phenylalanine ($pheA^{fbr}$) feedback-resistant genes

10.1021/bp0257473 CCC: $27.50
Published on Web 10/18/2003

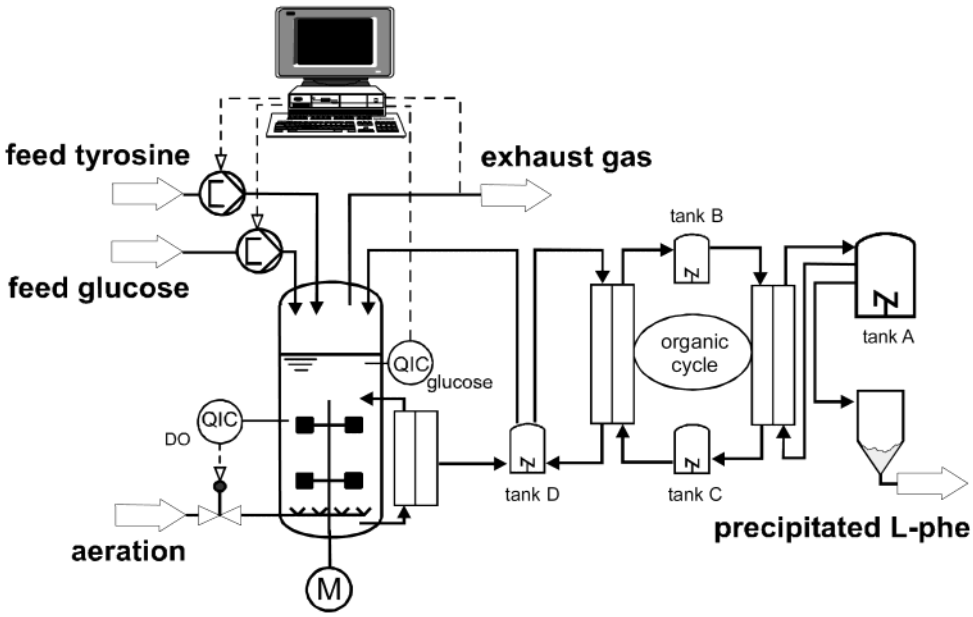

Figure 1. L-Phe process setup including the bioreactor for fed-batch L-Phe production with controlled glucose and tyrosine feed, ultrafiltration for biomass retention, and reactive-extraction with aqueous donor, acceptor, and organic kerosene/DEHPA cycle followed by a precipitation unit for L-Phe purification. Buffer tanks for donor (D), acceptor (A), and organic (B, C) phases are also shown.

were inserted on plasmid pF20 (based on pJF119EH) (Fürste et al., 1986) together with an ampicilline resistance gene. As a consequence of *tyrA* deletion, the production strain is tyrosine-auxotrophic. Induction is realized using IPTG.

Fermentation Conditions. Lab-scale fermentations were performed in a 20.0 L bioreactor (ISF 200, Infors, Switzerland) with an initial volume of 7.5 L, fermentation temperature of 37 °C, and pH 6.5 (controlled by 25% ammonia water); 15 g/L glucose (sole carbon source) and 0.3 g/L tyrosine were dissolved in the batch medium. To extend the growth phase, a glucose- (700 g/L) and tyrosine- (7.5 g/L) containing manual feed (see Figure 7) was started when glucose was reduced to 5 g/L. Later on, cell growth was limited at $OD_{620} \approx 80$ by installing a variable 700 g/L glucose feed that controls the glucose concentration at a constant 5 g/L level. At the same time, a limiting supply of 150 mg/h tyrosine was maintained. During the growth phase, L-Phe production was started by 100 μmol/L IPTG induction.

Pilot-scale fermentations were carried out in a 300 L Chemap bioreactor (Chemap, Switzerland) after a precultivation step using a 30 L bioreactor. The large-scale fermentation procedure was comparable to lab-scale fermentations except for the addition of 25 g/L tyrosine, which was now dissolved in 5% ammonia water (pH ~11) to avoid previously observed precipitation problems. As shown in Gerigk et al. (2002a), tyrosine feed was controlled by on-line oxygen-uptake measurements and its use in a heuristic controlling approach.

Further details of fermentation conditions, medium composition, etc. can be found in Gerigk et al. (2002a).

Reactive Extraction. As indicated in Figure 1, the reactive extraction unit, consisting of two hollow fiber modules (Liqui-Cell, Hoechst-Celanese Co., Charlotte, USA; effective membrane area 18.6 m^2) together with three 5 L tanks B, C, and D and a 50 L acceptor tank A, was fully integrated in the fermentation process. L-Phe-containing cell-free fermentation solution was pumped at decreasing rates from (initially) 22 to (later) 8 L/h from the ultrafiltration unit (500 kDa cutoff, 4.4 m^2 membrane area, 1 mm inner fiber diameter, Schleicher & Schuell, Germany) into the extraction module and was subsequently recycled into the bioreactor. The aqueous cell-free solution was brought into contact with the organic phase containing kerosene with 10 v/v % of the cation-selective carrier DEHPA (di-2-ethylhexyl-phosphonic acid). The proton exchange was assumed to take place in the aqueous phase next to the aqueous/organic interface as a result of the existing low aqueous carrier solubility (<1 g/L) and the nonsolubility of L-Phe cations in the organic phase. Loaded carrier/L-Phe complexes were transported to the back-extraction module, where L-Phe^+ was replaced by H^+ protons of H_2SO_4 source. Thus, an L-Phe concentration was realized in the aqueous acceptor phase that could be used for further product precipitation (titration with NaOH) as indicated. For further details of reactive-extraction conditions and the modules used see Maass et al. (2002).

For mass transfer studies, the reactive extraction unit of Figure 1 was used separately with circulating donor and acceptor streams. L-Phe concentration courses were monitored in the donor tank D ($c_{Phe,D}$) and in the acceptor tank A ($c_{Phe,A}$). During the experimental series the liquid streams of donor, acceptor, and organic phase varied from 60 to 680 L/h, which also caused different velocities inside the modules.

In the case of the aqueous phases, the velocity was calculated regarding the mean flow through the hydrophobic hollow fibers, whereas the velocity of the organic phase was estimated considering the mean flow through the outer space outside the fibers in the modules. Additionally the DEHPA (10−30% v/v) and the acid concentration (1−2 M) were changed. The set of 10 experiments is given in Table 1. The measured concentration courses of L-Phe in the acceptor and the donor are presented in Figures 3 and 4.

Analysis. To avoid unwanted glucose limitation, glucose was controlled at 5 g/L and measured on-line using an enzymatic online glucose analyzer (OLGA, IBA GmbH; Germany) together with a process control system called MEDUSA (in-house development) that includes a semi-continuous Kalman filter and a minimal-variance controller (MV3) as described in Gerigk et al. (2002a).

Table 1. Experimental Conditions of Mass Transfer Experiments. Flow Rates for Aqueous Donor ($\dot{V}_D$), Organic ($\dot{V}_O$), and Aqueous Stripping ($\dot{V}_A$) Phases and DEHPA and H_2SO_4 (c_{acid}) Concentrations

no.	$\dot{V}_D$ [L/h]	$\dot{V}_O$ [L/h]	$\dot{V}_A$ [L/h]	c_{DEHPA} [%, v/v]	c_{acid} [M]
1	250	156	500	10	1
2	240	156	680	10	1
3	250	60	500	10	1
4	250	60	250	10	1
5	250	60	250	20	1
6	250	60	250	20	2
7	250	60	250	30	1
8	250	156	250	20	2
9	500	156	250	20	2
10	250	156	250	30	2

Tyrosine was controlled via an indirect approach using a heuristic equation, which considers the oxygen uptake rate estimated on-line as an input variable.

Off-line analyses considered concentration measurements of (i) suspended cells using a spectrophotometer (Shimadzu UV-160, Germany) at 620 nm after appropriate dilution, (ii) cell dry weight (CDW) by filtration of 2.5−10.0 mL of fermentation broth through a preweighed microfilter (0.2 μm cutoff, Schleicher & Schuell, Germany), (iii) glucose by an enzyme-based biosensor appliance Accutrend (Roche Diagnostics, Mannheim, Germany), (iv) acetic acid by HPLC (Sycam, Germany) using an ion-exclusion column (Aminex-HPX-87H, BioRad, Germany) and a spectrophotometric detector at 215 nm (S3300, Sycam, Germany), and (v) amino acids (L-Phe and L-Tyr) by precolumn derivatization with the amino-specific reactant *o*-phthal-dialdehyde (OPA) and mercapto-ethanol followed by HPLC (Sycam, Germany) using a reversed-phase column (Lichrospher 100 RP 18-5 EC, Merck, Germany) and a fluorescence detector (RF-535, Shimadzu, Germany).

Modeling. Modeling was carried out using gPROMS 2.1.1 (Process System Enterprise Ltd., London, UK). As pointed out in the Introduction, it was a major aim of this study to identify a process model that is able to mirror the experimental results appropriately and that possesses a certain simplicity to encourage its easy use. For these reasons, no pH effects were considered in the model because the integrated process under consideration is assumed to be always performed at pH 6.5 owing to production strain qualities. Mass transfer modeling followed the idea of studying transfer kinetics in one hollow fiber and transferring the results by analogy to the whole bunch of fibers in the modules. As shown in Maass (2001), only very low concentration changes (<10%) occurred during a single flow of organic and aqueous solution through the hollow fiber modules, which is in agreement with further observations (Escalante et al., 1996) even studying opposite and nonopposite aqueous/organic flows. These experimental findings motivated the simplifying modeling assumption that nonopposite, parallel aqueous and organic streams could be assumed in the model in order to enable a straightforward parameter identification and to avoid complex recursive computing during nonlinear parameter identification. Hence, concentration changes along the hollow fibers (dependent on the variable *z*) are estimated expecting only small changes in accordance with former experimental observations. For model identification, the total set of concentration courses in acceptor and donor phase was used. Resulting mass transfer coefficients thus represent mean values with respect to process time, module length, and different experimental conditions.

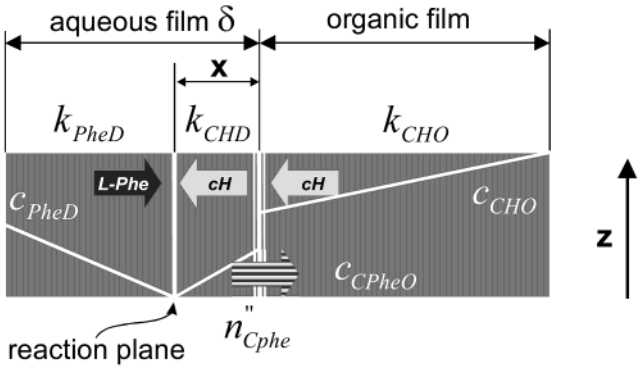

Figure 2. Modeling approach for the aqueous/organic L-Phe mass transfer. Carrier/H complexes of the organic phase are assumed to be transferred through the organic/aqueous interface to enter the aqueous film. By diffusion they are transported to a reaction plane, which is assumed to be located next to the interface where L-Phe is taken up and diffusively brought back to the interface, resulting in an area-specific carrier/Phe transfer called $\dot{n}''_{cPhe}$. All reactions and transport are in steady state.

Results and Discussion

Former mass transfer studies (Maass et al., 2002) indicated that simple "black-box" modeling approaches only provide limited insight into the mass transfer of the reactive-extraction unit and are thus not suitable to model and to design the total pilot-scale ISPR process. It turned out that the loading state of the carrier/L-Phe complex in the organic phase plays an important role during L-Phe separation. Unfortunately, concentrations of loaded or unloaded carriers could not be measured in the organic phase because appropriate analytical approaches were not available. Thus it was one aim of the modeling approach to estimate nonmeasurable carrier/L-Phe complex concentrations to discuss their affect on the total L-Phe mass transfer.

Mass Transfer Modeling. Detailed approaches for reactive-extraction modeling have been published, for instance by focusing on fundamentals of counter-transport under steady-state conditions (Kim and Stroeve, 1989) or by studying kinetic effects during L-Phe separation from aqueous solution using Aliquat 336 (Escalante et al., 1998). However, the experimental setup presented in this contribution (devices, extraction system, process integration, etc.) is not covered by these approaches. Moreover, it should be stressed that the following model considers the idea of a "reaction plane" to identify additional potential mass transfer limitations. This is motivated by the apparently low solubility of the carrier DEHPA, which contrasts with the good solubility of the often-used, cell toxic quaternary ammonium salt Aliquat 336, for which a modeling analysis was published by Escalante et al. (1998).

The modeling approach is based on the well-known "two-films theory" assuming an aqueous and an organic film that are directly in contact in the hollow fiber modules used. As indicated in Figure 2, all mass transfer rates are assumed to be in steady state, which means that the diffusively driven transport of carrier/proton-(H) complexes through the organic film equals their short-way diffusion through the aqueous film to the reaction plane (which is assumed to be located right next to the aqueous/organic interface) and also equals the counter diffusion of L-Phe cations coming from the bulk side of the aqueous film. The consideration of the reaction plane in the aqueous film is motivated by the existing (low) solubility of the carriers in the aqueous solution (together with the nonsolubility of L-Phe cations in the

organic phase) and allows the identification of potential mass transfer limitations caused by the low carrier solubility. Proton-exchange rates are known to be very fast (reaction rate constant 1.4×10^{11} L/mol·s (Atkins, 1996)), which consequently leads to thin reaction planes, from which newly produced carrier/L-Phe complexes diffuse back to the aqueous/organic interface. Rates and reactant concentrations (L-Phe in the donor phase, $c_{\mathrm{Phe,D}}$; carrier (DEHPA), c_{CHO}; and carrier/L-Phe complexes, C_{CPheO}, in the organic phase) are assumed to vary only slightly along the module (see modeling assumptions), which makes them dependent on the variable z. Corresponding mass transfer coefficients inside the films k_{PheD}, k_{CHD}, and k_{CHO} are defined with respect to the total module length (see Figure 2) and the total film thickness. At the aqueous/organic interface an equilibrium of carrier/proton(H) complexes in the organic phase with their counterparts in the aqueous phase is presumed. Focusing the L-Phe mass transfer near by the aqueous/organic interface, the steady-state assumption for all educts leads to the formulation of the area-specific L-Phe transfer rate $\dot{r}''(z)$:

$$\dot{r}''_{\mathrm{PheD}}(z) = k_{\mathrm{PheD}}(c_{\mathrm{PheD}}(z) - 0)\frac{\delta_{\mathrm{D}}}{\delta_{\mathrm{D}} - x} \tag{2a}$$

$$= k_{\mathrm{CHD}}(c_{\mathrm{CHD}}(z) - 0)\frac{\delta_{\mathrm{D}}}{x} \tag{2b}$$

$$= k_{\mathrm{CHO}}(c_{\mathrm{CHO}}(z) - c_{\mathrm{CHO,I}}(z)) \tag{2c}$$

Note that the educts are supposed to react completely at the reaction plane. The variable x is introduced to achieve a length-proportional reduction of the mass transfer coefficients and to allow a study of the presumed carrier-complex diffusion into the aqueous donor and into the acceptor phase. Because both reaction planes are assumed to be located right next to the organic/aqueous interface, $x \ll \delta_{\mathrm{D}}$. Further rearrangement of eqs 2a−c leads to

$$\dot{r}''_{\mathrm{PheD}}(z) = \frac{c_{\mathrm{CHOEx}}k_{\mathrm{CHD}} + c_{\mathrm{PheD}}k_{\mathrm{PheD}}K_{\mathrm{C}}}{\frac{k_{\mathrm{CHD}}}{k_{\mathrm{CHO}}} + K_{\mathrm{C}}} \tag{3}$$

where K_{C} describes an equilibrium constant taking into account the interface concentrations of the carrier/proton-(H) complex in organic and aqueous phase, which was experimentally estimated at 99.6 with the help of NMR measurements. It is worth noticing that eq 3 is only valid for $c_{\mathrm{CHOEx}} > 0 \cap c_{\mathrm{PheD}} > 0$.

By analogy, the modeling of the organic/aqueous mass transfer in the back-extraction module is realized

$$r''_{\mathrm{PheA}}(z) = \frac{c_{\mathrm{PheOBex}}k_{\mathrm{CPheA}} + c_{\mathrm{HA}}k_{\mathrm{HA}}K_{\mathrm{C}}}{\frac{k_{\mathrm{CPheA}}}{k_{\mathrm{CPheO}}} + K_{\mathrm{C}}} \tag{4}$$

considering the coefficients for mass transfer of the carrier/L-Phe complex in the aqueous acceptor phase, k_{CPheA}, and organic phase, k_{CPheO}, as well as proton(H) transport inside the aqueous acceptor phase, k_{HA}.

To model the complete experimental setup of Figure 1, the following differential equation system is used:

Extraction module:

L-Phe, aqueous:

$$\frac{\mathrm{d}c_{\mathrm{PheD}}(z)}{\mathrm{d}t} = -v_{\mathrm{D}}\frac{\partial c_{\mathrm{PheD}}(z)}{\partial z} - \frac{4}{D_{\mathrm{cap}}}r''_{\mathrm{PheD}}(z) \tag{5}$$

carrier/L-Phe, organic:

$$\frac{\mathrm{d}c_{\mathrm{CPheOEx}}(z)}{\mathrm{d}t} = -v_{O}\frac{\partial c_{\mathrm{CPheOEx}}(z)}{\partial x} + \frac{4}{D_{\mathrm{cap}}}r''_{\mathrm{PheD}}(z) \tag{6}$$

carrier/proton(H), organic:

$$c_{\mathrm{CHOEx}}(z) = c_{\mathrm{Const}} - c_{\mathrm{CPheOEx}}(z) \tag{7}$$

Back-extraction module:

L-Phe, aqueous:

$$\frac{\mathrm{d}c_{\mathrm{PheA}}(z)}{\mathrm{d}t} = -v_{\mathrm{A}}\frac{\partial c_{\mathrm{PheA}}(z)}{\partial z} + \frac{4}{D_{\mathrm{cap}}}r''_{\mathrm{PheA}}(z) \tag{8}$$

proton(H), aqueous:

$$\frac{\mathrm{d}c_{\mathrm{HA}}(z)}{\mathrm{d}t} = -v_{\mathrm{A}}\frac{\partial c_{\mathrm{PheA}}(z)}{\partial z} + \frac{4}{D_{\mathrm{cap}}}r''_{\mathrm{PheA}}(z) \tag{9}$$

carrier/L-Phe, organic:

$$\frac{\mathrm{d}c_{\mathrm{CPheOBex}}(z)}{\mathrm{d}t} = -v_{\mathrm{O}}\frac{\partial c_{\mathrm{CPheOBex}}(z)}{\partial z} - \frac{4}{D_{\mathrm{cap}}}r''_{\mathrm{PheA}}(z) \tag{10}$$

carrier/proton(H), organic:

$$c_{\mathrm{CHOBex}}(z) = c_{\mathrm{Cconst}} - c_{\mathrm{CPheOBex}}(z) \tag{11}$$

Additionally, four tanks must be considered (see Figure 1), leading to additional ordinary differential balance equations (see Appendix).

Modeling Results. Using this differential equation system, model identification was performed on the basis of the experimental data presented in Table 1 and in Figures 3 and 4. It turned out that of the six mass transfer coefficients initially considered, only two are necessary to model the experiments. While k_{CHD}, k_{CHO}, k_{CPheO}, and k_{HA} showed only poor statistical significance leading to typical over-parametrization problems (poor parameter accuracy $\gg$ 100%, singular parameter covariance matrix, etc.), the step-by-step model reduction finally lead to a reduced model that only consists of k_{PheD} and k_{CPheA} as model parameters. Table 2 shows high parameter accuracies by giving small relative standard deviations $\ll$ 1%.

Figures 3 and 4 represent an overview of the resulting model predictions compared to the experimental observations. It can be stated that the predicted concentration courses in the donor and acceptor tank are well mirrored by the model, which is indicated by high regression coefficients of L-Phe courses in the donor 0.983 ± 0.019 and acceptor tank 0.994 ± 0.005. This result might be surprising with respect to the significant simplifying assumptions which were the basis for model formulation. However it shows, that there obviously exists a small number of mass transfer limitations dominating the overall L-Phe transfer.

Motivated by the result that only k_{PheD} and k_{CPheA} were revealed to be significant under different experimental conditions, the conclusion can be formulated that in the extraction module neither the transport of carrier/proton-(H) complexes in the organic phase nor their short-way diffusion in the aqueous phase is limiting, but obviously

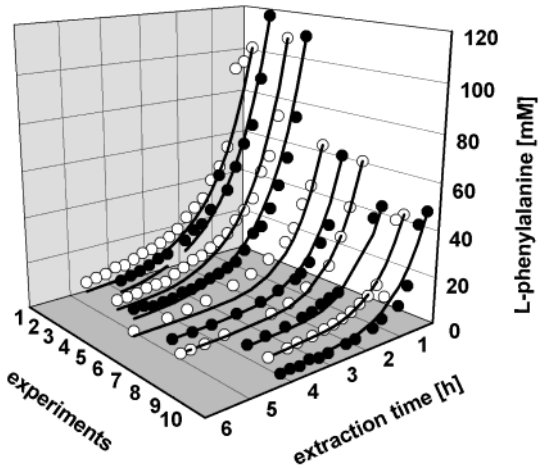

Figure 3. Modeled and measured (decreasing) L-phenylalanine courses of all 10 experiments in the aqueous donor phase in buffer tank D, which was connected to the extraction module.

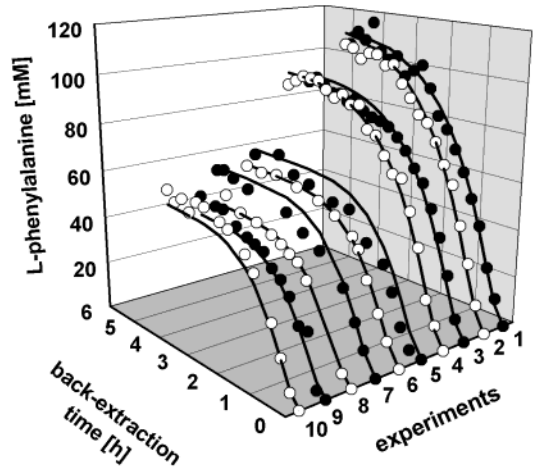

Figure 4. Modeled and measured (increasing) L-phenylalanine courses of all 10 experiments in the aqueous acceptor phase in buffer tank A, which was connected to the back-extraction module.

Table 2. Final Parameters of L-Phe Mass Transfer Model Identified from the 10 Pilot-Scale Experiments Presented in Table 1

parameter	unit	value	sd
k_{pheD}	cm/s	128×10^{-7}	≪1%
k_{CPheA}	cm/s	178×10^{-5}	≪1%

the L-Phe diffusion in the aqueous film is the most significant transfer step. k_{PheD} is estimated at 128×10^{-7} cm/s. By analogy it is assumed that in the back-extraction module no significant limitation of the carrier/Phe-complex transport, as well as of the proton(H), exists. However, the transfer of L-Phe-loaded carriers into the aqueous acceptor phase seems to be limiting. Here a mass transfer coefficient k_{CPheA} of 178×10^{-5} cm/s was estimated. The mass transfer coefficients differ in 2 orders of magnitude. This is most presumably a consequence of the significantly different L-Phe concentrations in the corresponding phases, which is compensated by different mass transfer coefficients under the constraint of steady-state flux.

The fact that no mass transfer limitation is identified in the organic phase might be surprising, especially if lower diffusivity for the carrier/L-Phe complex and extensive laminar films in the organic phase are expected. However, one should consider the very low solubility of the carrier/L-Phe complex in the aqueous phase, which is 2 orders of magnitude smaller than in the organic phase and which consequently limits the mass transfer. The model identification results based on the different experimental conditions (see Table 1) and the accuracy of model predictions support this simple mass transfer model. Additional mass transfer studies focusing on the aqueous/organic interface would be desirable; however, they could not be performed within this project.

Macrokinetic Model of the L-Phe-Producing Strain. To study whether and how the reactive extraction model can be used for total process modeling, a complete ISPR approach together with the fed-batch fermentation process has to be formulated. To enable a comparison of pure simulation and large-scale experiments, the fermentation model was identified using a different database, namely, a small-scale fed-batch process. It was the general aim to keep the macrokinetic approach as simple as possible, which resulted in the following nonsegregated, nonstructured approach:

$$\mu = \mu_{max} \frac{c_{Tyr}}{c_{Tyr} + K_{STyr}} \tag{12}$$

$$\sigma_{Tyr} = m_{Tyr} + \frac{\mu}{Y_{xTyr}} \tag{13}$$

$$\pi_{Phe} = \pi_{Phemax} \frac{K_{lPhe}}{K_{lPhe} + c_{Phe}} \tag{14}$$

It is assumed that the growth of L-Phe-producing *E. coli* cells is only dependent on the (limiting) supply of the auxotrophic amino acid tyrosine, because glucose concentrations were controlled at a saturating level of 5 g/L during the whole fermentation (see preceding). A tyrosine maintenance consumption is considered (see eq 13). L-Phe production is supposed to be completely growth-decoupled but inhibited by high product concentrations as observed with respect to AroF activity. The macrokinetic model was used together with ordinary differential balancing equations (not shown) taking the concentrations of cell-dry weight (c_{CDW}), L-Phe (c_{Phe}), tyrosine (c_{Tyr}), and the liquid volume (V_R) as dependent variables and considering the common feed of glucose and tyrosine as an independent input variable.

Figure 5 presents a comparison of modeled and measured values. The model parameters are given in Table 3. Only a poor estimation of Y_{XTyr} and m_{Tyr} can be stated, thus leading to a temporary inaccurate model prediction of tyrosine consumption, σ_{Tyr}. The inaccuracies are the consequence of experimental difficulties caused by partial tyrosine precipitation that occurred inside the feed tubing owing to the very low tyrosine solubility of 0.38 g/L. However, the modeling of the L-Phe course is not hampered, which is most important for the ongoing studies. Note that a significant L-Phe inhibition constant of 20 ± 1.35 g/L is identified, confirming previous AroF inhibition results.

Modeling the Total Process. Combining the fermentation model with the reactive-extraction modeling approach, a total process model is identified aiming at the simulation of the 300 L fed-batch L-Phe production with fully integrated L-Phe separation on a pilot-scale as described in Gerigk et al. (2002a). Figure 6 compares simulated and measured values of L-Phe concentration in the bioreactor and in the acceptor tank together with the bioreactor tyrosine course. Additionally the glucose/

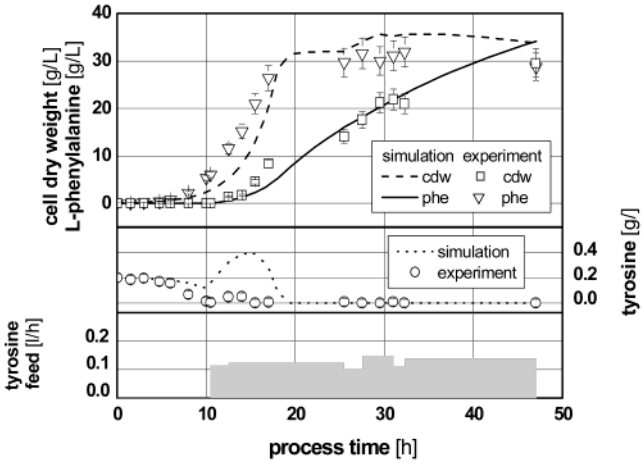

Figure 5. Comparison of modeled and measured values of cell dry weight (cdw), L-phenylalanine (phe), tyrosine (tyr), and the tyrosine feeding rate in a lab-scale fermentation process using an L-Phe-producing *E. coli* strain.

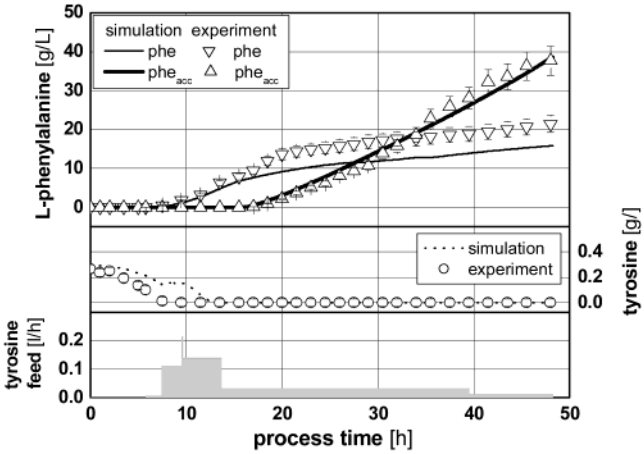

Figure 6. Simulation of the total L-Phe production process based on the model parameters, which were identified separately. Shown are the concentration courses of measured and simulated L-phenylalanine in the bioreactor (Phe) and in the acceptor tank of reactive extraction (Phe_{acc}), together with the corresponding values of tyrosine (Tyr) in the fermentation suspension during the fed-batch process. Additionally, the tyrosine feed is given.

Table 3. Parameters of the Macrokinetic Model Identified from One Fed-Batch Lab-Scale Fermentation for L-Phe Production Using a Recombinant *E. coli* Strain As Described

parameter	unit	value	sd
μ_{max}	L/h	0.321	±0.01127
K_{STyr}	g/L	0.00152	$\pm 2.53 \times 10^{-6}$
Y_{xTyr}	g_{CDW}/g_{Tyr}	35.29	>100%
m_{Tyr}	$g_{Tyr}/g_{CDW}h$	0.00245	>100%
π_{Phemax}	$g_{phe}/g_{CDW}h$	0.0756	±0.049
K_{IPhe}	g_{phe}/L	20	±1.35

tyrosine feeding profile is given. As indicated in Figure 1, the reactive-extraction was combined with the fed-batch process via an ultrafiltration unit, of which the permeate rates were taken as independent (measured) input variables for the simulations varying between 22 and 8 L/h (caused by bio-fouling that occurred during filtration).

Figure 6 indicates a good conformity between measured and simulated courses; in particular the L-Phe accumulation in the acceptor tank is well reflected by the model predictions. Thus, the conclusion is drawn that the simple

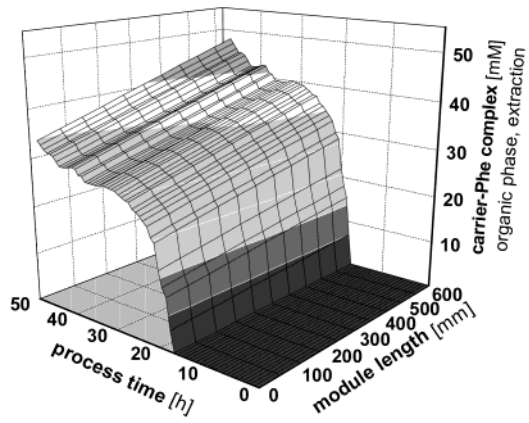

Figure 7. Simulated course of the carrier/L-Phe complex in the organic phase in the extraction module as a function of process time and module length during the on-line reactive extraction of L-Phe from the fed-batch process on the 300 L scale.

ISPR model is applicable to model the overall process. This offers the possibility to study the nonmeasurable carrier/L-Phe complex in the organic phase taking into account the modeled values (see Figure 7).

As an example, the three-dimensional plot of the carrier/L-Phe complex in the extraction module is given in Figure 7. It can be seen that reactive-extraction started after 13.6 h and lasted until the end of the process at 48 h. Surprisingly, the simulation reveals that still loaded carrier re-enter the extraction module, causing a significant accumulation of the carrier/L-Phe complex in the organic phase up to 45 mM at the outlet after 48 h. This result is especially remarkable as there was no alternative analytical approach to measure the loaded carrier/L-Phe fraction in the organic phase. Furthermore, the accumulation of the loaded carrier/L-Phe complex can be regarded as a potential candidate of existing mass transfer limitations, which need to be studied in detail.

Optimization of the ISPR Process. As a consequence, one might think of increasing the back-extraction membrane area to reduce the amount of still-loaded carriers re-entering the extraction unit. Thus, corresponding simulations were carried out by increasing the number of back-extraction modules, installed in series, from one to three. As indicated in Figure 8, the concentration of still-loaded carriers re-entering the extraction module decreased significantly, as was previously assumed. However, the rate of L-Phe transfer, which is monitored at the entrance of the back-extraction module, did not increase as expected. In contrast, a decrease of L-Phe transfer is found by increasing the number of extraction modules used.

This result might be surprising at first sight; however, taking into account the identified main transfer limitations, namely, k_{PheD} and k_{CPheA}, a phenomenological explanation can be given.

The identification of k_{PheD} indicates that L-Phe mass transfer inside the extraction module is only dependent on the mass transfer of L-Phe cations through the aqueous film to the reaction plane and not on the carrier/L-Phe complex in the organic phase inside the module. Hence, extraction rates are independent of the back-extraction membrane area (data not shown). In contrast, back-extraction rates are significantly reduced because of reduced carrier/L-Phe concentrations in the organic phase. Decreasing carrier/L-Phe concentrations in the organic phase also cause decreasing carrier/L-Phe con-

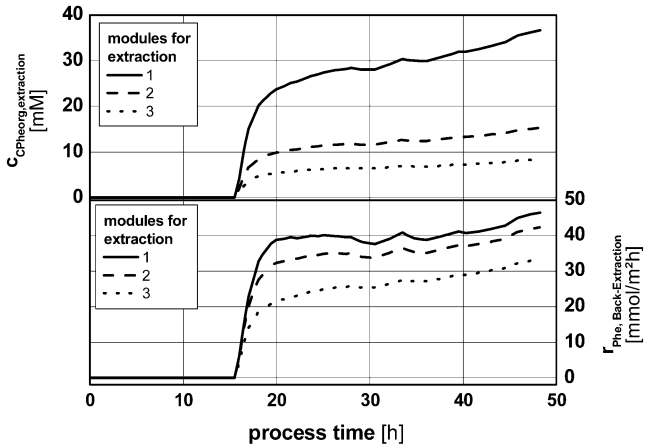

Figure 8. Comparison of the concentration [mM] of the carrier/L-Phe complex at the entrance of the extraction module with the resulting L-Phe mass transfer rates [mmol/m²h] mirrored at the entrance of the back-extraction module. Both variables are presented as functions of process time. Three simulation runs are shown for each variable, considering up to three similar back-extraction modules installed in series.

centrations in the aqueous acceptor phase, which are most significant for total back-extraction (indicated by k_{CPheA}).

This analysis reveals the complexity of the total L-Phe mass transfer and consequently stresses the need to perform corresponding simulation studies. As shown, there are obviously two major limitation steps that were found inside the aqueous films regarding the L-Phe cations in the donor and the carrier/L-Phe complex in the acceptor phase. As a consequence, the following strategies for total process optimization can be discussed:

(i) If k_{PheD} is focused, high L-Phe concentrations in the permeate (and also in the fermentation broth) are advantageous. With respect to the identified product inhibition of 20 g/L, there obviously exists an upper limit to follow this route for process optimization. However, one can think of a later start of the reactive-extraction unit during the process run, provided that the further product accumulation does not exceed critical L-Phe titers. Furthermore, the use of optimized L-Phe producers (with higher production rates) can also be considered. Here, the use of on-line L-Phe separation would be most advantageous to prevent a fast accumulation of the inhibiting product.

(ii) By analogy, the mass transfer described by k_{CPheA} can be discussed, leading to simulation studies with extended extraction membrane area or considering alternative carriers, which possess higher aqueous solubility and which are still tolerated by the cells.

(iii) Finally, one should consider that all identified candidates for mass transfer limitations are located in the films of the aqueous phase. These films originate from the laminar conditions inside the hollow fiber modules. Hence, the optimization of the integrated reactive extraction could also focus on the improvement of hydrodynamics at the organic/aqueous interface in order to minimize aqueous film extension and to eliminate corresponding transfer limitations subsequently.

Conclusion

Summing up the modeling studies, a simple process model is identified that is suitable to mirror experimental observations of the total ISPR process and allows the formulation of some basic strategies for further process optimization. These will be investigated in future experiments. Furthermore, the model represents a valuable basis for the economic evaluation of the ISPR approach, which of course is necessary to implement a further scale-up to a large-scale production process.

Acknowledgment

The author would like to thank the former Ph.D. students Dr. M. Gerigk and Dr. D. Maass for providing the data used in the modeling analysis presented and Dr. A. A. de Graaf (MetabolicExplorer GmbH, Jülich, Germany) for performing NMR measurements. The author would also like to thank DSM Biotech GmbH for their fruitful cooperation and co-financing together with the German Federal Ministry of Education and Research (Grant 0311644). Last but not least, the author wants to express his thanks to Prof. C. Wandrey for providing optimum working conditions at the Institute of Biotechnology, Research Centre Juelich, Germany.

Appendix

In addition to the above-mentioned ODEs, the following mass balances are used to model concentration courses in the buffer tanks B and C, in the donor tank D, and in the acceptor tank A. Please notice that index 0 and L refer to the entrance and to the exit of the hollow fiber modules. For the sake of brevity only L-Phe balances are given.

Acceptor tank A

$$\frac{dc_{PheA}(0)}{dt} = \frac{\dot{V}_A}{V_A}(c_{PheA}(L) - c_{PheA}(0))$$

Buffer tank B

$$\frac{dc_{CPheOBex}(0)}{dt} = \frac{\dot{V}_O}{V_B}(c_{CPheOEx}(L) - c_{CPheOBex}(0))$$

Buffer tank C

$$\frac{dc_{CPheOEx}(0)}{dt} = \frac{\dot{V}_O}{V_C}(c_{CPheOBex}(L) - c_{CPheOEx}(0))$$

Donor tank D

$$\frac{dc_{PheD}(0)}{dt} = \frac{\dot{V}_D}{V_D}(c_{PheD}(L) - c_{PheD}(0))$$

Notation

c_{Cconst}	total amount of carrier in the organic phase, constant (mmol/L)
c_{HA}	proton concentration in the aqueous acceptor phase (mmol/L)
c_{CHD}	carrier/proton complex concentration at the organic/aqueous interface (mmol/L)
c_{CHO}	carrier/proton complex concentration in the organic bulk (mmol/L)
c_{CHOBex}	carrier/proton complex concentration in the organic bulk in the back-extraction module (mmol/L)
c_{CHOEx}	carrier/proton complex concentration in the organic bulk in the extraction module (mmol/L)
$c_{CHO,I}$	carrier/proton complex concentration at the organic/aqueous interface (mmol/L)
c_{Phe}	L-Phe concentration in the fermentation suspension (mmol/L)

c_{PheA} L-Phe concentration in the bulk of the acceptor phase (mmol/L)

c_{PheD} L-Phe concentration in the bulk of the aqueous phase (mmol/L)

$c_{CPheOBex}$ carrier/proton complex concentration in the organic bulk in the back-extraction module (mmol/L)

$c_{CPheOEx}$ carrier/L-Phe concentration in the organic bulk in the extraction module (mmol/L)

D_{cap} outer diameter of the hollow fibers (m)

δ_D thickness of the aqueous film in the donor phase (m)

K_C equilibrium constant between the interface concentration of the carrier complex in organic and aqueous phase, estimated experimentally

k_{CHD} mass transfer coefficient of carrier/proton complex from the aqueous organic interface to the reaction plane inside the aqueous film of the donor phase (m/s)

k_{CHO} mass transfer coefficient of carrier/proton complex from the organic bulk to the organic/aqueous interface inside the organic film (m/s)

k_{CPheA} mass transfer coefficient of the carrier/Phe complex from the aqueous/organic interface to the reaction plane inside the aqueous film of the acceptor phase (m/s)

k_{CPheO} mass transfer coefficient of the carrier/Phe complex from the bulk of the organic phase to the organic/aqueous interface inside the organic film (m/s)

k_{HA} mass transfer coefficient of protons from the bulk to the reaction plane inside the aqueous film of the acceptor phase (m/s)

K_{lPhe} inhibition constant with respect to L-Phe (mmol/L)

k_{PheD} mass transfer coefficient of L-Phe from the bulk to the reaction plane inside the aqueous film of the donor phase (m/s)

m_{Tyr} maintenance of tyrosine consumption (mmol/(g_{cdw}h))

μ specific growth rate (L/h)

μ_{max} maximum specific growth rate (L/h)

π_{Phe} biomass specific L-Phe product formation (mmol/(g_{cdw} h))

π_{Phemax} maximum biomass specific L-Phe product formation (mmol/(g_{cdw} h))

$\dot{r}''_{PheA}$ area specific L-Phe flux at the aqueous acceptor and organic interface (mmol/(m^2s))

$\dot{r}''_{PheD}$ area specific L-Phe flux at the aqueous donor and organic interface (mmol/(m^2s))

σ_{Tyr} biomass specific tyrosine consumption rate (mmol/(g_{cdw}h))

$\dot{V}_A$ liquid acceptor stream (L/h)

$\dot{V}_D$ liquid donor stream (L/h)

$\dot{V}_O$ liquid organic stream (L/h)

V_A volume of acceptor tank (L)

V_B volume of upper buffer tank in organic cycle (L)

V_C volume of lower buffer tank in organic cycle (L)

V_D volume of donor tank (L)

v_A average velocity of the aqueous acceptor phase inside the hollow fibers of the back-extraction modules (m/s)

v_D average velocity of the aqueous donor phase inside the hollow fibers of the extraction modules (m/s)

Y_{xTyrr} biomass/tyrosine yield (g_{cdw}/mmol)

x distance between reaction plane and aqueous organic interphase, is assumed to be located close to the interface (M)

References and Notes

Atkins P. W. *Physical Chemistry*, 5th ed,; Oxford University Press: New York, 1994.

Bongaerts, J.; Krämer, M.; Müller, U.; Raeven, L.; Wubbolts, M. Metabolic Engineering for Microbial Production of Aromatic Amino Acids and Derived Compounds. *Metab. Eng.* **2001**, *3*, 289−300.

Budzinski, A. Aminosäuren, Peptide und die Chemie dazu. Chemische Rundschau 6, 10, ISSN 0009-2983, 2001.

Calorie Control Council; Low-Calorie Sweeteners: Aspartame; www.caloriecontrol.org/aspartame.html, 2002.

Drauz, K. H.; Hoppe, B.; Kleemann, A.; Krimmer, H. P.; Leuchtenberger, W.; Weckbecker, C. Amino Acids. In *Ullmann's Encyclopedia of Industrial Chemistry*, 6th ed.; Wiley-VCH: Weinheim, Germany, 2002.

Escalante, H.; Ortiz, M. I.; Irabien, J. A. Concentration of L-Phenylalanine by Nondispersive Extraction in Hollow Fibre Modules. ISEC 96, Melbourne, Australia, 2002, 1493−1498.

Escalante, H.; Alonso, A. I.; Ortiz, I.; Iarabien A. Separation of L-Phenylalanine by Nondispersive Extraction and Back-extraction. Equilibrium and Kinetic Parameters. *Sep. Sci. Technol.* **1998**, *33*(1), 119−139.

Fürste, J. P.; Pansegrau, W.; Frank, R.; Blöcker, H.; Scholz, P.; Bagdasarian, M.; Lanka, E. Molecular Cloning of the Plasmid RP4 Primase Region in a Multi-Host-Range tacP Expression Vector. *Gene* **1986**, *48*, 119−131

Gerigk, M. R.; Maass, D.; Kreutzer, A.; Sprenger, G.; Bongaerts, J.; Wubbolts, M.; Takors R. Enhanced Pilot-Scale Fed-Batch L-Phenylalanine Production with Recombinant *Escherichia coli* by Fully Integrated Reactive Extraction. *Bioprocess Biosyst. Eng.* **2002a**, *25*, 43−52.

Gerigk, M. R.; Bujnicki, R.; Ganpo-Nkwenkwa, E.; Bongaerts, J.; Sprenger, G.; Takors, R. Process Control for Enhanced L-Phenylalanine Production Using Different Recombinant *E. coli* Strains. *Biotechnol. Bioeng.* **2002b**, *80*(7), 746−754.

Kim, J.-I.; Stroeve, P. Uphill Transport in Mass Separation Devices With Reactive Membranes: Counter-Transport. *Chem. Eng. Sci.* **1989**, *44*(5), 1101−1111.

Maass, D. Prozessentwicklung zur simultanen Produktabtrennung von L-Phenylalanin. Ph.D. Thesis, Berichte des Forschungszentrum Jülich. ISSN 0944−2952, 2001.

Maass, D.; Gerigk, M. R.; Kreutzer, A.; Weuster-Botz, D.; Wubbolts, M.; Takors, R. Integrated L-Phenylalanine Separation in an *E. coli* Fed-Batch Process: From Laboratory to Pilot Scale. *Bioprocess Biosyst. Eng.* **2002**, *25*, 85−96.

Müller, A. Hartes Gerangel um den Futtertrog. Chemische Rundschau 6, 1, ISSN 0009-2983, 2001.

Accepted for publication September 16, 2003.

BP0257473